

Many-Beam Solution to the Phase Problem in Crystallography

Christoph T. Koch^{1,*}

¹Max Planck Institute for Metals Research, Heisenbergstr. 3, 70569 Stuttgart, Germany

(Dated: June 9, 2018)

Solving crystal structures from electron diffraction patterns rather than X-ray diffraction data is hampered by multiple scattering of the fast electrons within even very thin samples and the difficulty of obtaining diffraction data at a resolution high enough for applying direct phasing methods. This letter presents a method by which the effect of multiple scattering is being used for solving the phase problem, allowing the retrieval of electron structure factors from diffraction patterns recorded with varying angle of incidence without any assumption about the scattering potential itself. In particular, the resolution in the diffraction data does not need to be sufficient to resolve atoms, making this method particularly interesting for electron crystallography of 2-dimensional protein crystals and other beam-sensitive complex structures.

PACS numbers: 61.05.jd, 61.05.jm, 61.05.cc

Electron crystallography becomes the method of choice when trying to determine the atomic structure of small crystalline volumes for mainly 2 reasons: a) electrons can be focused into sub-nanometer probes, and b) their scattering strength is about 4 orders of magnitude greater than that of X-rays. For structure determination of inorganic materials the strong interaction of electrons with the scattering medium is traditionally being viewed as a nuisance because existing methods for solving the phase problem in X-ray crystallography assume kinematic scattering, making these methods generally not directly applicable to electron diffraction intensities. Solving the structure of 2-dimensional protein crystals from electron diffraction data alone, on the other hand, is hampered by that fact that these beam-sensitive samples do not generally provide data of sufficient resolution to satisfy the preconditions for kinematic phasing methods.

Recently, approaches which use the sensitivity of multiply scattered X-rays to structure factor phases have proven useful [1, 2, 3]. The comparatively flat Ewald sphere describing the scattering of high energy electrons usually causes more than just 3 reflections to be close to the Bragg condition, especially in complex structures, making these methods generally inapplicable for phase determination from electron diffraction data. Also in the field of low energy electron diffraction (LEED) dynamical scattering is being applied for solving the phase problem [4].

Without loss of generality it is assumed that the specimen surface normal is parallel to the zone axis as well as the z -axis, as illustrated in figure 1. The deviation of the 3-dimensional wave vector of the incident electron beam $\vec{k} = (k_x, k_y, k_z) = (\vec{k}_t, k_z)$ from the z -axis is then usually quite small. Based on the Bloch wave solution to the Klein-Gordon equation of high energy scattering of a fast incident beam electron by the crystal potential [8, 9] the intensity $I_{g_n}(\vec{k}_t)$ of any point in the diffraction pattern defined by the reciprocal lattice vector \vec{g}_n of the particular diffraction spot and the tangential component

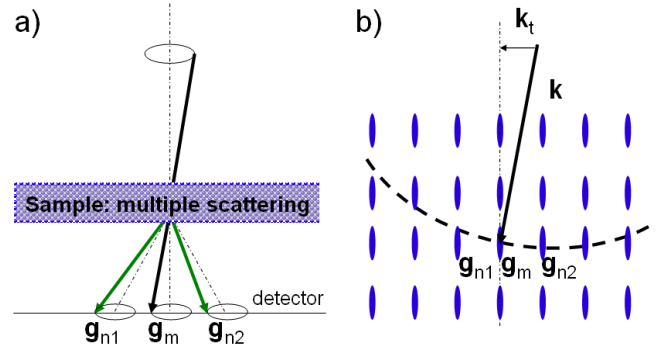


FIG. 1: Diagram illustrating the relevant parameters in real (a) and reciprocal space (b). a) In convergent beam electron diffraction (CBED) experiments diffraction patterns for all incident beam directions whose \vec{k}_t -component lie within a disc are recorded. b) The reciprocal space representation illustrates how changing the incident beam direction causes the Ewald sphere (dashed arch) to intersect the crystal potential reciprocal lattice rods (REL rods) with varying excitation errors.

of the incident electron wave vector \vec{k}_t is given by the modulus squared of the element of the scattering matrix

$$S(\vec{k}_t)_{n,m} = [e^{iT A}]_{n,m} \quad (1)$$

in the n^{th} row and the "central beam" column m , i.e. the beam index m for which the reciprocal lattice vector $\vec{g}_m = 0$. Here A is a square matrix with the potential energy terms $A_{n,m} = U_{\vec{g}_n - \vec{g}_m}$ as its off-diagonal elements and the (relativistically corrected) terms $\xi_n = -(|\vec{g}_n|^2 + 2\vec{g}_n \cdot \vec{k})/\gamma$ related to the kinetic energy part of the modified Schroedinger equation along its diagonal.

The scalar parameter $T = \pi\gamma\lambda t$ depends on the wavelength $\lambda = (\lambda_0^{-2} + U_0)^{-1/2} \approx \lambda_0$ of the incident electron beam corrected by the mean potential U_0 of the crystal, the specimen thickness t , and the relativistic correction factor $\gamma = 1 + |e|v/m_0c^2$ (here m_0 and e are rest mass and

charge of the electron and v is the accelerating voltage).

Note that I did not multiply the electron structure factors $U_{\vec{g}_n - \vec{g}_m} = 2m_0|e|V_{\vec{g}_n - \vec{g}_m}/h^2$ ($V_{\vec{g}} = \Omega^{-1} \int_{\text{cell}} V(\vec{r}) \exp(2\pi i \vec{g} \cdot \vec{r}) d^3 \vec{r}$ are the Fourier coefficients of the crystal potential $V(\vec{r})$, where the integration is over one unit cell, and Ω is the unit cell volume) in A with the usual relativistic correction factor γ but included it in T instead, in order to separate true material constants ($U_{\vec{g}}$) from variable experimental parameters ($\lambda(v), \gamma(v), t, \vec{k}_t$). The additive constant of U_0 for every element along the diagonal of A has also been omitted because it only produces a general attenuation of the diffraction pattern due to its imaginary part and a global phase offset due to the real part of U_0 , both immeasurable in a conventional diffraction experiment.

The crystal potential $V(\vec{r}) = V^r(\vec{r}) + iV^i(\vec{r})$ consists of a real part describing the elastic scattering and an imaginary part accounting for inelastic scattering processes which produce a non-isotropic attenuation in the scattered signal, if we collect the zero-loss scattered electrons only, as is routinely done in today's quantitative (energy filtered) electron diffraction experiments. This means that even for centro-symmetric crystals the $U_{\vec{g}}$ are in general complex, and have a non-zero phase.

It has been shown that the Bloch wave expression (1) can be expanded in a "scattering path" or Born series [10], providing a very general expression which agrees with those derived earlier by analyzing the multiple scattering process directly [11, 12, 13]. Reference [10] provides a recursive, but finite explicit expression for the coefficients $C_{n,l_1,\dots,l_{q-1},m}^q(T, \vec{k}_t)$ in the expansion

$$|S(T, \vec{k}_t)_{n,m}|^2 = |e^{T\xi_n(\vec{k}_t)} \delta_{n,m} + \underbrace{\sum_{q=1}^{\infty} \sum_{l_1=0}^N \sum_{l_2=0}^N \cdots \sum_{l_{q-1}=0}^N}_{q} U_{\vec{g}_n - \vec{g}_{l_1}} U_{\vec{g}_{l_1} - \vec{g}_{l_2}} \cdots U_{\vec{g}_{l_{q-1}} - \vec{g}_m} C_{n,l_1,\dots,l_{q-1},m}^q(T, \vec{k}_t)|^2 \quad (2)$$

for arbitrary scattering path lengths, even in the (degenerate) case of multiple excitation of the same reflection. The interested reader is referred to the original publication [10], where the complete expression along with its derivation is provided.

The complex product of any two scattering path coefficients $c_{n,l_1,\dots,l_{q_1-1},h_1,\dots,h_{q_2-1}}^{q_1,q_2}(T, \vec{k}_t) = C_{n,l_1,\dots,l_{q_1-1},m}^{q_1}(T, \vec{k}_t) \cdot C_{n,h_1,\dots,h_{q_2-1},m}^{q_2}(T, \vec{k}_t)^*$ defines scale and phase factor with which any $q_1 + q_2 = q$ -monomial of structure factors $U_{\vec{g}_n - \vec{g}_{l_1}} \cdots U_{\vec{g}_{l_{q_1-1}} - \vec{g}_m} U_{\vec{g}_n - \vec{g}_{h_1}}^* \cdots U_{\vec{g}_{h_{q_2-1}} - \vec{g}_m}^*$ contributes to the diffraction intensity in the beam g_n .

The convergence of above scattering path expansion (3) depends on the value of $T = \pi\gamma\lambda t$ and the modulus of the largest structure factor. Increasing the specimen thickness or decreasing the accelerating voltage will

therefore increase the largest order of significant monomials in the expansion. We will let q_{max} be the length of the longest scattering path - or, in other words, the largest order of monomial - included in the expansion from here on. The coefficients $c^{q_1,q_2} = c^{q_1,q_2}(T, \vec{k}_t)$ ($q_1 + q_2 \leq q_{max}$, I will omit the functional dependence for increased readability from here on) depend in addition to the specimen thickness and accelerating voltage also on the easily variable experimental parameters \vec{k}_t . Measuring diffraction intensities for a set of different values of incident electron beam tilt \vec{k}_t , as in a convergent beam electron diffraction (CBED) experiment, allows a system of coupled multi-variate polynomial equations of degree q_{max} to be defined whose solution is the set of structure factors which best (in a least squares sense) describe the observed intensities for the set of experimental parameters. The resulting system of equations can be solved by the reformulation-linearization technique [14] which has been proven to converges to a global optimum.

In order to keep the size of the set of polynomial equations within manageable limits T should be small enough to let the first term in the expansion, the kinematic scattering intensity at reflection \vec{g}_n , $n \neq m$,

$$I_{g_n}^{(2)}(T, \vec{k}_t) = |C_{n,m}^1(T, \vec{k}_t) U_{g_n}|^2 = \left| \frac{e^{T\xi_n} - 1}{\xi_n} U_{g_n} \right|^2 = c_n^{1,1} |U_{g_n}|^2 = \frac{\gamma^2 \sin^2(\pi\lambda t S_{g_n})}{S_{g_n}^2} |U_{g_n}|^2 \quad (3)$$

($S_{g_n} = \frac{1}{2}\xi_n/\gamma$ is also called the excitation error) be the dominant contribution, at least to the strong reflections. Although the kinematic scattering approximation $I_{g_n}^{(q_{max}=2)}$ is not sensitive to any structure factor phase invariants, it allows us to define sensible limits on the structure factor amplitude.

It also provides a very simple way of determining the specimen thickness, the only unknown parameter in the c^{q_1,q_2} coefficients (accelerating voltage and incident beam tilt can usually be controlled very precisely). By fitting the (normalized) experimental 2-dimensional rocking curves $I_{g_n}(\vec{k}_t)$ for all reflections with the kinematical one $I_{g_n}^{(2)}(T, \vec{k}_t)$ given by expression (3), both, the specimen thickness as well as a first estimate for the structure factor amplitude can be obtained. The form of expression (3) allows this fit to be implemented very efficiently as a simple one-parameter search in the specimen thickness t . The structure factor amplitudes are then determined directly for each trial value of t . This is, by the way a much more precise measurement of structure factor amplitudes than using the integrated rocking curve as is done in precession electron diffraction [15].

Setting $q_{max} = 3$ the scattering intensity at reflection \vec{g}_n ($n \neq m$) becomes

$$I_{g_n}^{(3)}(T, \vec{k}_t) = c_n^{1,1} |U_{g_n}|^2 + \sum_l c_{n,l}^{2,1} U_{\vec{g}_n - \vec{g}_l} U_{\vec{g}_l} U_{g_n}^* +$$

$$\begin{aligned} & \sum_k c_{n,h}^{1,2} U_{\vec{g}_n} U_{\vec{g}_n - \vec{g}_h}^* U_{\vec{g}_h}^* \\ &= I_{g_n}^{(2)}(T, \vec{k}_t) + 2\text{Re} \left[\sum_l c_{n,l}^{2,1} U_{\vec{g}_n - \vec{g}_l} U_{\vec{g}_l} U_{\vec{g}_n}^* \right] \end{aligned}$$

The monomials $U_{\vec{g}_n - \vec{g}_l} U_{\vec{g}_l} U_{\vec{g}_n}^*$ can be written as the product of the 3 structure factor amplitudes and a phase factor whose argument is the 3-phase invariant $\phi_{\vec{g}_n - \vec{g}_l} + \phi_{\vec{g}_l} - \phi_{\vec{g}_n}$, indicating that $I_{g_n}^{(3)}(T, \vec{k}_t)$ must also be sensitive to these phase invariants.

The reformulation-linearization technique developed by Sherali and Tuncbilek [14] converts the non-linear polynomial equations into linear ones by treating each monomial as an independent variable. By defining additional linear equations that result from obvious relationships between the monomials as well as inequalities produced by upper and lower bounds on the variables the polynomial set of equations is converted into a set of linear equalities and inequalities for which a solution can be found, if one exists, using standard linear programming algorithms. Once a solution has been found, the limits on the variables may be readjusted ("branch and bound"), resulting in a new linear programming problem and eventually the global solution.

If the initial estimate of the structure factor amplitudes is fairly reliable, the limits within which the correct structure factor amplitude must lie may be defined very tightly. It is then very likely that the correct solution will be found already in the first linearization step, as has been the case for the test case described below.

In order to verify the performance of the phase retrieval method described above it has been tested using simulated electron diffraction data. Since it has already been shown that Friedel asymmetries in dynamical diffraction patterns of non-centrosymmetric structures can be used to solve the phase problem [16], I used simulated diffraction patterns of Si in the (110) projection, a simple centro-symmetric structure for demonstration purposes. If absorption is neglected, as has been done for this test case, kinematic and higher order scattering contributions to the diffraction intensities cannot be separated simply on the basis of their symmetry, as it is partly the case for non-centro-symmetric structures [16], making the reconstruction of centro-symmetric structures even more challenging.

Recently, a TEM-controlling software has been developed in our laboratory (and tested on a Zeiss EM 912 and the Zeiss SESAM [18]) that allows automated acquisition of energy-filtered pseudo-large angle CBED (pseudo-LACBED) patterns to be recorded on either slow-scan CCD camera or imaging plates [17]. The advantage of pseudo-LACBED patterns over conventional CBED patterns is that, although the radius of each individual diffraction disc may be several reciprocal lattice vectors, discs produced by the different diffraction spots do not

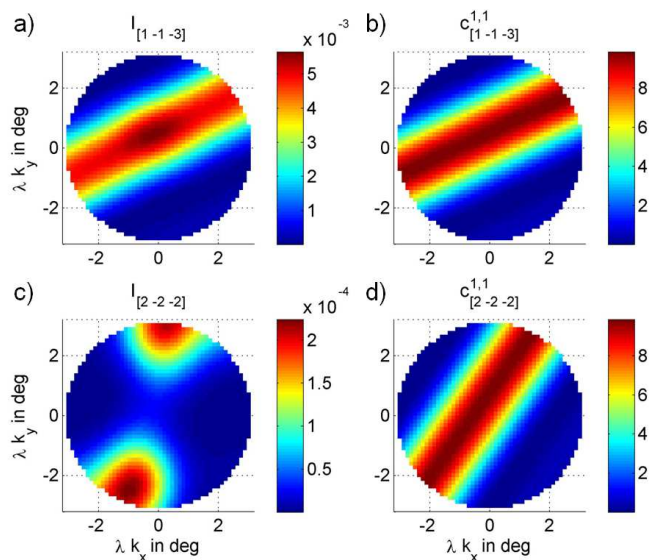


FIG. 2: a) Simulated LACBED disc for $\vec{g} = [1\bar{1}\bar{3}]$. b) The coefficient $c_{[1\bar{1}\bar{3}]}^{1,1}(t = 3.985\text{nm}, \vec{k}_t)$ given by expression 3 (unscaled kinematic rocking curve). The square root of the proportionality constant between the 2 plots in a) and b) provides a first estimate of the structure factor amplitude for this reflection. c) Simulated LACBED disc for the kinematically forbidden reflection $[2\bar{2}\bar{2}]$. Comparing the diffraction intensity of a forbidden reflections with the corresponding kinematic rocking curve (d) allows its identification to be automated.

overlap and may therefore be recorded in a single exposure. This apparently unphysical effect is produced by scanning (and, below the specimen, partially descanning) the angle of incidence of a nearly parallel beam during the exposure of the recording medium. The large disc radius is necessary to observe fluctuations in the diffraction intensities across the discs despite the low sample thickness required to keep dynamical diffraction effects at a moderate level. For light matter (e.g. protein crystals) the sample thickness may actually be quite high, drastically reducing the need to use very large convergence angles.

LACBED disc intensities for the following 27 beams have been computed by Bloch wave simulation: $[\bar{2}22]$, $[\bar{2}\bar{2}\bar{2}]$, $[00\bar{2}]$, $[\bar{3}31]$, $[\bar{3}\bar{3}\bar{1}]$, $[\bar{2}24]$, $[\bar{2}\bar{2}\bar{4}]$, $[\bar{1}13]$, $[\bar{1}\bar{1}\bar{3}]$, $[004]$, $[\bar{2}20]$, $[\bar{1}11]$, $[\bar{1}\bar{1}\bar{1}]$, $[000]$, $[111]$, $[\bar{1}\bar{1}\bar{1}]$, $[220]$, $[004]$, $[\bar{1}13]$, $[\bar{1}\bar{1}\bar{3}]$, $[\bar{2}24]$, $[\bar{2}\bar{2}\bar{4}]$, $[\bar{3}\bar{3}\bar{1}]$, $[\bar{3}\bar{3}\bar{1}]$, $[002]$, $[\bar{2}22]$, $[\bar{2}\bar{2}\bar{2}]$. An accelerating voltage of 200 kV, a specimen thickness of 4 nm and a disc radius of 3° have been used, a beam tilt angle which is easily achievable in actual experiments with the acquisition method described in the previous paragraph.

Examples of the resulting diffraction data are shown in figure 2 a and c. While the high symmetry of centrosymmetric structures removes potentially useful Friedel asymmetries in the diffraction data, it also imposes sym-

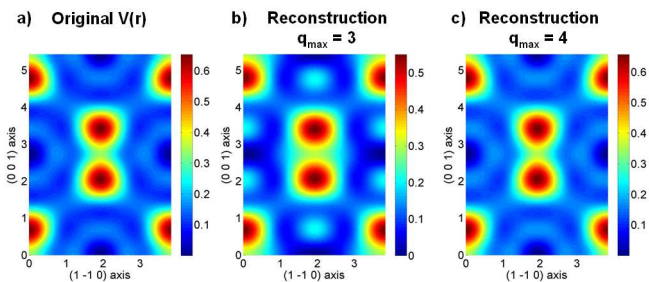


FIG. 3: Reconstructed real-space potential distribution within a single unit cell of Si in the (110) projection. a) Potential distribution used to simulate the diffraction data. b) Reconstruction from a scattering path expansion with $q_{max} = 3$, i.e. one scattering order beyond the kinematic approximation. It is quite obvious that this order of approximation is not sufficient. c) Reconstruction from a scattering path expansion with $q_{max} = 3$ showing excellent agreement with the original. Since the value of U_0 cannot be reconstructed from the available data, the potential is displayed with its minimum value set to 0 in all 3 figures.

metry constraints on the structure factors themselves. The 26 structure factors corresponding to the reflections listed above are reduced to 8 independent real-values variables (U_0 was set to 0 for reasons mentioned earlier).

In step 1 of the reconstruction the specimen thickness and initial estimates of the structure factor amplitudes were obtained by fitting kinematic rocking curves (see figure 2 b and d) to the simulated pseudo-LACBED discs by nonlinear single parameter least-squares fitting w.r.t. the specimen thickness as described earlier, automatically removing forbidden reflections from the fit based on their poor agreement with the shape of the kinematic rocking curves. The best matching thickness was found to be 3.985 nm, deviating only 0.3 from the thickness used for the simulation, most likely due to dynamical effects.

In step 2 of the reconstruction the previously determined sample thickness of 3.985 nm was used to define the $c_{g_n}^{q_1, q_2}(T, \vec{k}_t)$ coefficients. Both, the definition of these coefficients as well as the setup of the linearized system of polynomial equations is fully automated, requiring as only input the specimen thickness, the reciprocal lattice vectors to be included in the reconstruction, the deviation from zone axis \vec{k}_t for each point within the LACBED discs and the diffraction intensity at that point. All of these parameters can be obtained directly from the (calibrated) diffraction pattern.

In step 3 of the reconstruction the previously defined system of linear equations and inequalities was solved using the lsqin function provided by the Matlab optimization toolbox, which applies an active set method for solving linear programs in its medium-scale version. Repeating the reconstruction for $q_{max} = 3$ and $q_{max} = 4$ resulted in the projected potential plots shown in figures

3b and 3c respectively. The reconstruction for $q_{max} = 4$ involved 33 different monomials, 11670 equalities and 122 inequalities and took about 1 second on a 2.2 GHz laptop equipped with 500 MB RAM to compute, solving for magnitude and sign of 6 distinct structure factors (being equal to zero, the structure factors of the forbidden reflections had been removed automatically from the fit in step 1 of the reconstruction).

The agreement of the second reconstruction including scattering paths up to length 4 with the original potential is excellent, demonstrating that this method works very well, provided that scattering paths of sufficiently high order are included. Increasing the number of reflections increases the number of unknowns, but also the number of available data. However, the number of monomials, equalities and inequalities increases as the q_{max}^{th} power of the number of structure factors to be determined. It will therefore be necessary to define a scheme by which the dominant monomials and the linear relationships between them will be kept, discarding those which are not important - a path currently being pursued.

In summary, a new method for solving the inversion problem of dynamical scattering from (convergent beam electron) diffraction data from moderately thin samples has been presented. Apart from the usually well-defined accelerating voltage the data required by the reconstruction may be directly obtained from the diffraction pattern. No assumptions are being made about the scattering potential within a single unit cell, making this method much more general than direct phasing methods applied to kinematical diffraction data. The method uses dynamical scattering effects in the diffraction data to solve directly for the structure factor amplitudes and phases.

Although the application of this method to X-ray diffraction patterns is quite conceivable, it is expected that its main application will be in the field of structural electron crystallography. Simulated pseudo-LACBED data of Si (110) has been used to test this method.

I want to thank Prof. H. D. Sherali for his very helpful suggestions on how to solve multivariate polynomial sets of equations.

* koch@mf.mpg.de

- [1] S. L. Chang, Phys. Rev. Lett. **48**, 163-166 (1982)
- [2] H. Juretschke, Phys. Rev. Lett. **48**, 1487-1489 (1982)
- [3] Q. Shen, Phys. Rev. Lett. **80**, 3268-3271 (1997)
- [4] D.K. Saldin, A. Seubert, K. Heinz, Phys. Rev. Lett. **88**, 115507 (2002)
- [5] L. J. Allen, T.W. Josefsson, and H. Leeb, Acta Cryst. **A54**, 388-398 (1998)
- [6] J. C. H. Spence, B. Calef, and J.M. Zuo, Acta Cryst. **A55**, 112-118 (1999)
- [7] P. Rez, Acta Cryst. **A55**, 160-167 (1999)
- [8] F. Fujimoto, J. Phys. Soc. Japan **14**, 1558 (1959)

- [9] C. J. Humphreys, Rep. Prog. Phys. **42**, 1825-1885 (1979)
- [10] C. T. Koch, and J. C. H. Spence, Journal of Physics A: Mathematical and General **36**, 803-816 (2003)
- [11] J. M. Cowley, and A. F. Moodie, Acta Cryst. **10**, 609-619 (1957)
- [12] K. Fujiwara, Journ. Phys. Soc. Japan **14**, 1513-1524 (1959)
- [13] A. F. Moodie, Z. Naturforsch **27**, 437-440 (1972)
- [14] H. D. Serali and C. H. Tuncbilek, Journal of Global Optimization **2**, 101-112 (1992)
- [15] R. Vincent and P. A. Midgley, Ultramicroscopy **53**, 271 (1994)
- [16] C. T. Koch, Acta Cryst. A **61**, 231-236 (2005)
- [17] C. T. Koch, P. Bellina, P. A. van Aken, Proceedings of the 14th European Microscopy Congress 2008 in Aachen, Vol. II, p. ??
- [18] C. T. Koch, W. Sigle, R. Höschel, M. Rühle, E. Essers, G. Benner and M. Matijevic, Microscopy and Microanalysis **12**, 506-514 (2006)